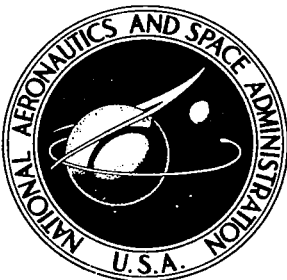


NASA CR-1842

NASA CONTRACTOR
REPORT



NASA CR-1842

C.1

00901031



TECH LIBRARY KEEF, NM

LOAN COPY: RETURN TO
AFWL (DOGL)
KIRTLAND AFB, N. M.

A SHOCK WAVE STUDY
OF COCONINO SANDSTONE

by F. H. Shipman, V. G. Gregson, and A. H. Jones

Prepared by

GENERAL MOTORS CORPORATION

Warren, Mich. 48090

for Ames Research Center

NATIONAL AERONAUTICS AND SPACE ADMINISTRATION • WASHINGTON, D. C. • MAY 1971



0061011

1. Report No. NASA CR-1842	2. Government Accession No.	3. Recipient's Catalog No.	
4. Title and Subtitle A Shock Wave Study of Coconino Sandstone		5. Report Date May 1971	
7. Author(s) F. H. Shipman, V. G. Gregson and A. Jones		6. Performing Organization Code	
9. Performing Organization Name and Address General Motors Corporation Manufacturing Development Warren, Michigan 48090		8. Performing Organization Report No.	
12. Sponsoring Agency Name and Address National Aeronautics & Space Administration Washington, D.C. 20546		10. Work Unit No.	
		11. Contract or Grant No. NAS 2-3427	
		13. Type of Report and Period Covered Contractor Report	
		14. Sponsoring Agency Code	
15. Supplementary Notes			
16. Abstract Hugoniot equation of state measurements to 1400 kb were made on Coconino sandstone. This data is summarized with other quartz shock wave data and used to estimate isotherms for the three solid phases of quartz, coesite and stishovite. Calculations of shock temperature have been made based on these isotherms and lead to an estimation of the phase boundaries of quartz polymorphs under dynamic loading. The dynamic phase boundaries are shown to shift significantly compared to those determined statically.			
17. Key Words (Suggested by Author(s)) Hugoniot equation of state, Coconino sandstone, quartz, coesite, stishovite, shock-wave	18. Distribution Statement UNCLASSIFIED-UNLIMITED		
19. Security Classif. (of this report) UNCLASSIFIED	20. Security Classif. (of this page) UNCLASSIFIED	21. No. of Pages 47	22. Price* 3.00



TABLE OF CONTENTS

	<u>Page</u>
LIST OF ILLUSTRATIONS	iv
LIST OF TABLES	v
INTRODUCTION	1
SECTION I - SHOCK WAVE DATA	3
SECTION II - PRESSURE-VOLUME PHASE DIAGRAM FOR QUARTZ	13
SECTION III - TEMPERATURE CALCULATIONS	22
CONCLUSIONS	38
APPENDIX - HUGONIOT STANDARDS	41
LITERATURE CITED	42

LIST OF ILLUSTRATIONS

<u>Figure</u>		<u>Page</u>
1	Shock Velocity versus Particle Velocity for GM Data on Coconino Sandstone	6
2	GM Hugoniot for Coconino Sandstone	7
3	Shock Velocity versus Particle Velocity Data of Sandstone	9
4	Hugoniot for Sandstone Data	10
5	(a) Idealized Models of Polymorphic Phase Transformation (b) Having Transition Times Less Than and (c) Greater Than the Risetime of the Shock Front	14
6	(a) Idealized Models of Polymorphic Phase Transformation of a (b) Solid and (c) Porous Material Having a Transition Time Greater Than the Risetime of the Shock Front	16
7	Interpretation of Solid and Porous Quartz Hugoniots	18
8	Pressure-Volume Phase Diagram for Quartz	19
9	Low-Strain Rate Phase Diagram for Quartz	23
10	Coconino Sandstone Hugoniot Showing Pressure Regions Used for Temperature Calculations	27
11	Specific Heat Capacity as a Function of Temperature for α -Quartz, β -Quartz, Tridomite and Cristobalite	28
12	Specific Heat Capacity as a Function of Temperature for Coesite and Stishovite	29
13	Solid Quartz Hugoniot Showing Pressure Regions Used for Temperature Calculations	36
14	High Strain Rate Phase Diagram for Quartz	37

LIST OF TABLES

<u>Table</u>		<u>Page</u>
I	Physical Properties of Coconino Sandstone	4
II	Hugoniot Data for Coconino Sandstone	5
III	Low Strain Rate Data for Equilibrium Phase Diagram of Quartz (Figure 9)	24

INTRODUCTION

Various forms of quartz have long been studied and constitute an important body of information for geologists and geophysicists. Quartz is a ubiquitous mineral. It is a major constituent of many sedimentary rocks and an important component in some igneous and metamorphic rocks. The polymorphism, stability and reaction kinetics of quartz in several of its six forms is important in concepts of the mineralogy and physical properties of the earth's interior. An example is some of the several possible stable phase assemblages or transformations of feldspar between 30 and 200 kb:

1. Oligoclase \rightarrow jadeite + gossularite + kyanite + SiO_2 (quartz, coesite, stishovite). James (1969).
2. Microcline \rightarrow hollandite. Ringwood, Reid and Wadsley (1967).

The density of the first assemblage depends upon the thermodynamic state of quartz. In turn, these phase assemblages might be used in more elaborate models of the mantel which must be consistent with density variations within the mantle.

This report describes and presents the results of a study of shock wave loading of Coconino sandstone from Meteor Crater, Arizona. These results extend and add to previous work described by Jones, et al. (1968); Ahrens and Gregson (1964); and Gregson and Grine (1963). Combining the results of these

workers, we attempt to describe the polymorphism of quartz (i.e., α -quartz, coesite, stishovite) under high rates of loading at high pressures. The hugoniot of sandstone leads us to believe that mixed regions of both α -quartz/coesite and α -quartz/stishovite do exist at high rates of loading not only in sandstone but also in crystalline quartz as well.

Experimental techniques employed in the present work to achieve high pressures are described in detail elsewhere (Jones, et al., 1968 and Shipman, et al., 1968). The technique involves the use of an accelerated reservoir light gas gun to launch a flat plate of one of several metals with well-documented shock wave properties. Metal plates are made to strike an instrumented specimen and the data parameters of the shock wave are recorded. This technique allows the generation of pressure states higher than previously attained through the conventional use of explosives because impact velocities as high as 8 km/sec are obtained.

Conversion of recorded data to pressure-volume states in the shock front is possible by using precise measurement of the impactor velocity and shock wave velocity in the specimen together with the known hugoniot equation of state of the impactor. The Rankine-Hugoniot conservation equations are then used to calculate the pressure-volume and energy state behind the shock wave front in the sample.

SECTION I

SHOCK WAVE DATA

The physical properties of Coconino sandstone tested in this study are presented in Table I. The general petrologic description and physical properties of this Coconino sandstone are nearly identical to those reported by Ahrens and Gregson (1964). Measurements of the acoustic velocities using a pulse transmission overlap technique are included for further completeness of material characterization.

A total of 17 experiments were performed using an accelerated reservoir light gas gun facility. Measurements of hugoniot shock states in Coconino sandstone ranged from about 40 to 1400 kb. This range of shock states was achieved by varying the launch velocity of the flat plate impactor from approximately 1 to 8 km/sec and using impactors of varying shock impedances. The experimental techniques will be discussed below in aspects related to data comparison.

Data presented in Table II are also displayed in Figures 1 and 2 showing shock velocity-particle velocity and pressure-specific volume relationships respectively. Data tolerances and error bars are included to illustrate the scatter recorded at each represented shock state.

The simplest representation of hugoniot data as a description of behavior in shock velocity-particle velocity coordinates (U_s , u_p). A least squares analysis is used to fit a smooth

TABLE I
PHYSICAL PROPERTIES OF
COCONINO SANDSTONE

Mineral Composition

97% Quartz
3% Feldspar
Trace Clay and Heavy Minerals

Grain Size

Average and Modal Grain Size - 0.117 - 0.149 mm
Range of Grain Diameters 0.062 - 0.71 mm

Density

Bulk Density - 1.98 gm/cm³
Grain Density - 2.67 gm/cm³

Porosity (Calculated)

25%

Strength

Unconfined Crushing Strength normal to bedding
 3.14×10^8 dynes/cm² dry, 3.64×10^8 dynes/cm²
saturated with water (block size 2.2 X 2.2 X 5 cm).

Sonic Velocities

Longitudinal C_L = 4.188 km/sec \pm .08 (Vacuum Dry)
Shear C_S = 2.68 km/sec \pm .3 (Vacuum Dry)

Description

Specimen is weakly to moderately well cemented with silica, in the form of quartz overgrowths on the grains. Subparallel laminae 5.0 to 17.5 mm thick are separated by thin laminae 0.5 mm thick containing more than average amounts of silt and clay sized grains. A petrofabric study of C-axis orientations can be found in Gregson and Grine, (1963).

TABLE II
HUGONIOT DATA FOR CONCONINO SANDSTONE

$$\rho_0 = 1.98 \pm .03 \text{ gm/cc}$$

<u>Impactor Material and Velocity</u> (km/sec)	<u>Remarks</u>	<u>Shock Velocity</u> (km/sec)	<u>Particle Velocity</u> (km/sec)	<u>Shock Pressure</u> (Mb)	<u>Specific Volume</u> (cc/gm)	<u>Shot No.</u>
Cu .851	No Shim	2.95±.12	.74	.043±.002	.378±.005	S-241
Cu 1.211	Wedge Exper. 2.5-12.5mm	3.20±.06	1.039	.066±.001	.341±.003	S-257
Cu 1.588	5.84	3.674±.001	1.330	.0968	.3222	S-153
Cu 1.965	5.84	4.10	1.63	.132	.304	S-156
Cu 2.054	5.84	4.269±.002	1.700	.1437	.3040	S-247
Cu 2.650	5.84	4.49±.10	2.18	.194±.004	.260±.005	S-1127
Cu 3.155	5.84	4.84±.02	2.57	.246±.001	.237±.002	S-152
Cu 3.528	5.84	5.25±.02	2.86	.297±.001	.230±.001	S-239
Cu 3.898	5.84	5.66±.01	3.12	.349±.001	.227±.001	S-154
Cu 4.063	5.84	5.79±.04	3.25	.373±.002	.222±.005	C-1128
Cu 5.540	5.84	7.57±.03	4.30	.644±.003	.218±.002	C-1130
Cu 5.731	5.84	7.79±.14	4.43	.684±.011	.218±.010	C-1179
Cu 6.642	5.84	8.72±.06	5.07	.875±.006	.211±.002	S-160
Cu 6.652	* 5.84mm	8.82±.03	5.07	.886±.003	.215±.003	S-158
Cu 6.662	* 4.63mm	9.08±.01	5.05	.908±.002	.224±.001	S-159
Cu 7.895	* 3.94mm	10.09	5.94	1.187	.208	S-155
FS-77 7.871	*	11.20	6.43	1.426	.215	S-157

* Shim Thickness = .082mm Brass

FS-Fansteel-77

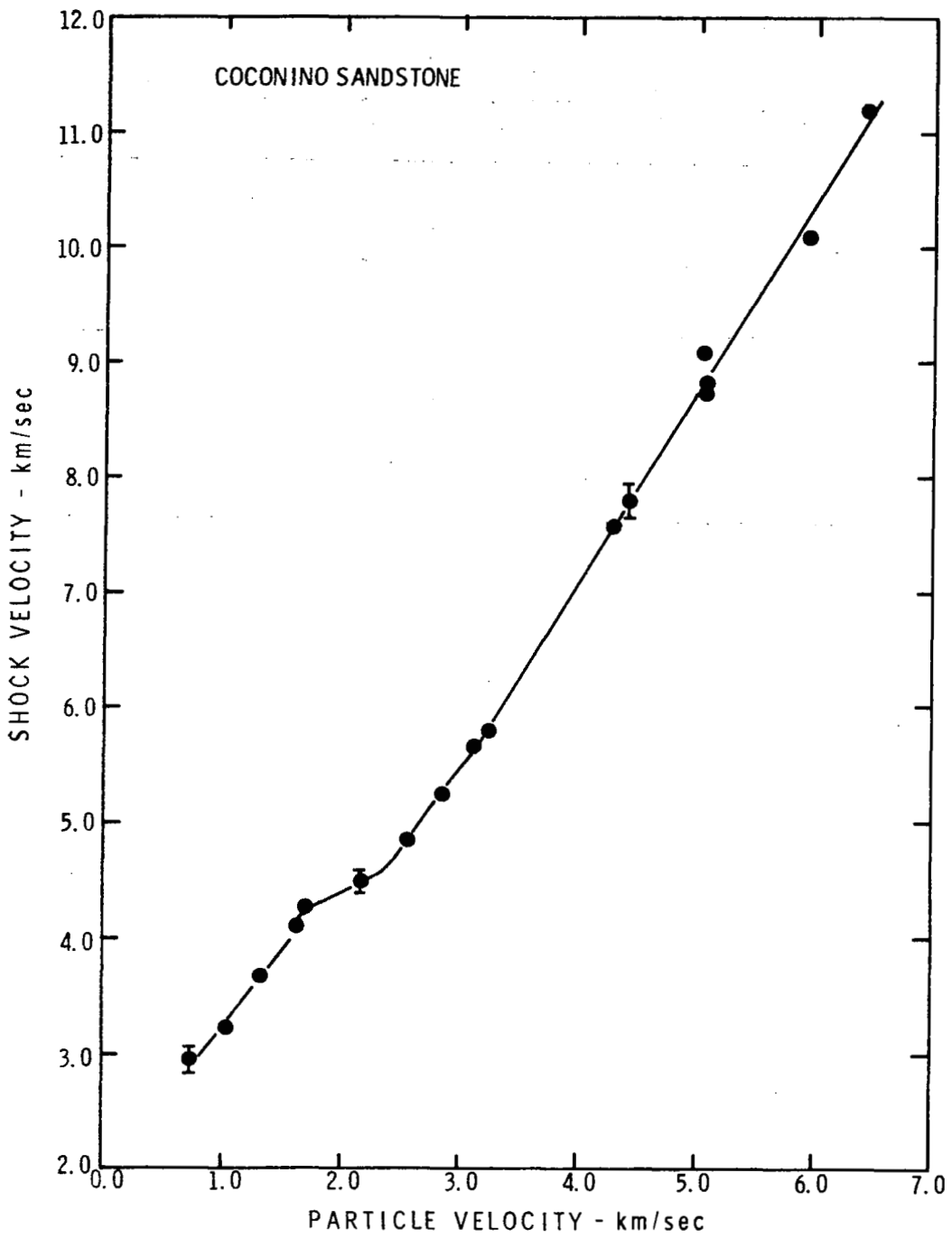


Figure 1 Shock Velocity versus Particle Velocity
for GM Data on Coconino Sandstone

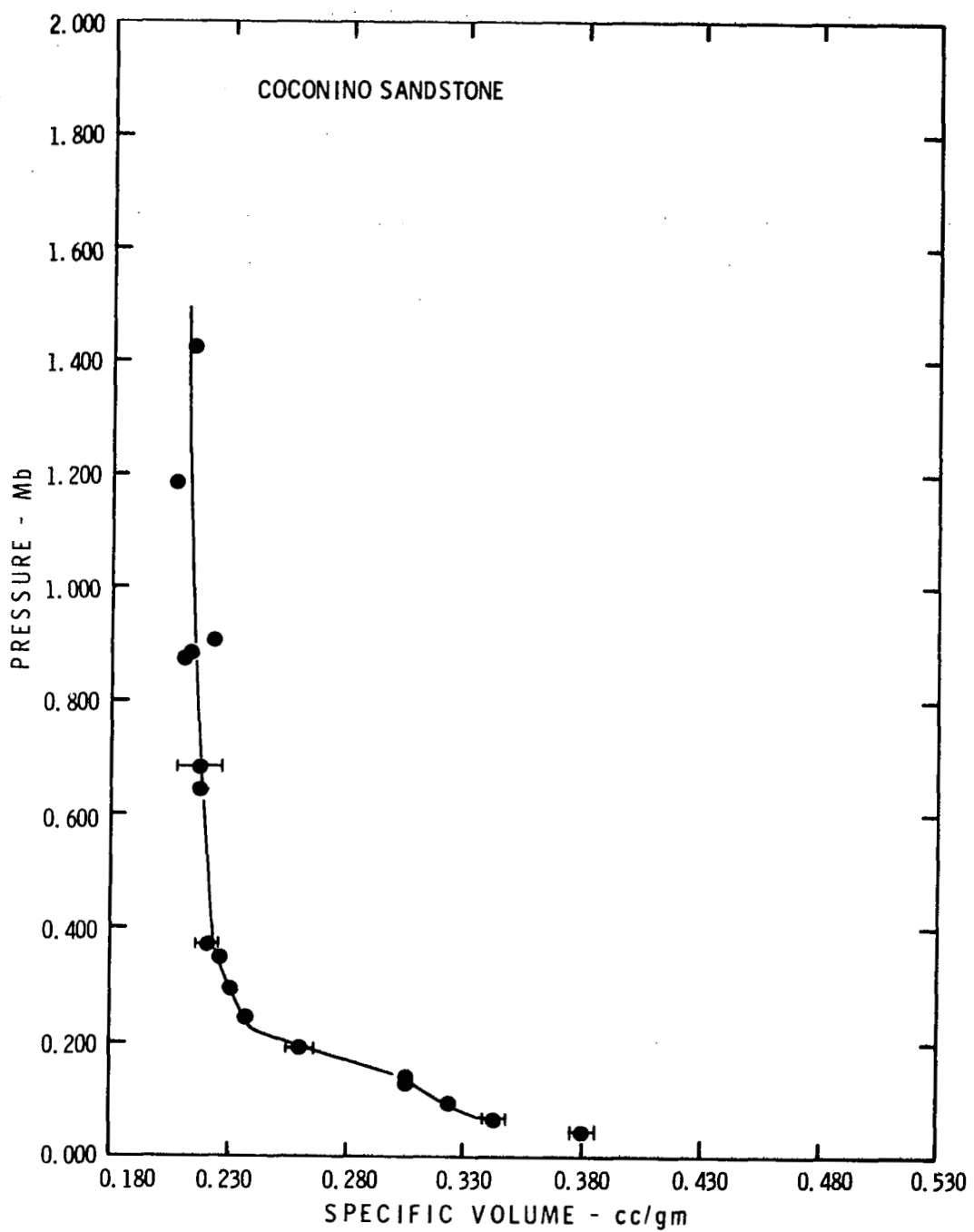


Figure 2 GM Hugoniot for Coconino Sandstone

curve to the $U_s - u_p$ data. Most commonly, a linear function of the form $U_s = C_0 + S u_p$ is employed as an auxillary equation of state which allows interpolation between data. Where discontinuities are evident, linear line segments are here employed for the same purpose but only over the range of particle velocities of the segment. In general, but not necessarily, departures from linearity are evidence of changes in structural behavior e.g. plastic failure, melting, polymorphism in shock loaded materials (McQueen, et al., 1967).

Comparison of the shock velocity-particle velocity and pressure-specific volume data of Ahrens and Gregson (1964) and this work is made in Figures 3 and 4 showing our interpretation of these data.

Region I represents the elastic behavior of sandstone established by Ahrens and Gregson (1964) where the HEL (Hugoniot Elastic Limit) was measured to between 4.1 to 5.1 kb.

The next two regions use the data from the HEL (Hugoniot Elastic Limit) as determined by Ahrens and Gregson (1964) and lower data points reported here.

REGION II

$$U_s = 1.751 + 1.495 u_p \text{ km/sec}$$

$$0.3 < u_p < 0.8 \text{ km/sec} \quad \text{Std. Error of } U_s = 0.103 \text{ km/sec}$$

REGION III

$$U_s = 1.380 + 1.652 u_p \text{ km/sec}$$

$$0.95 < u_p < 1.8 \text{ km/sec} \quad \text{Std. Error of } U_s = 0.112 \text{ km/sec}$$

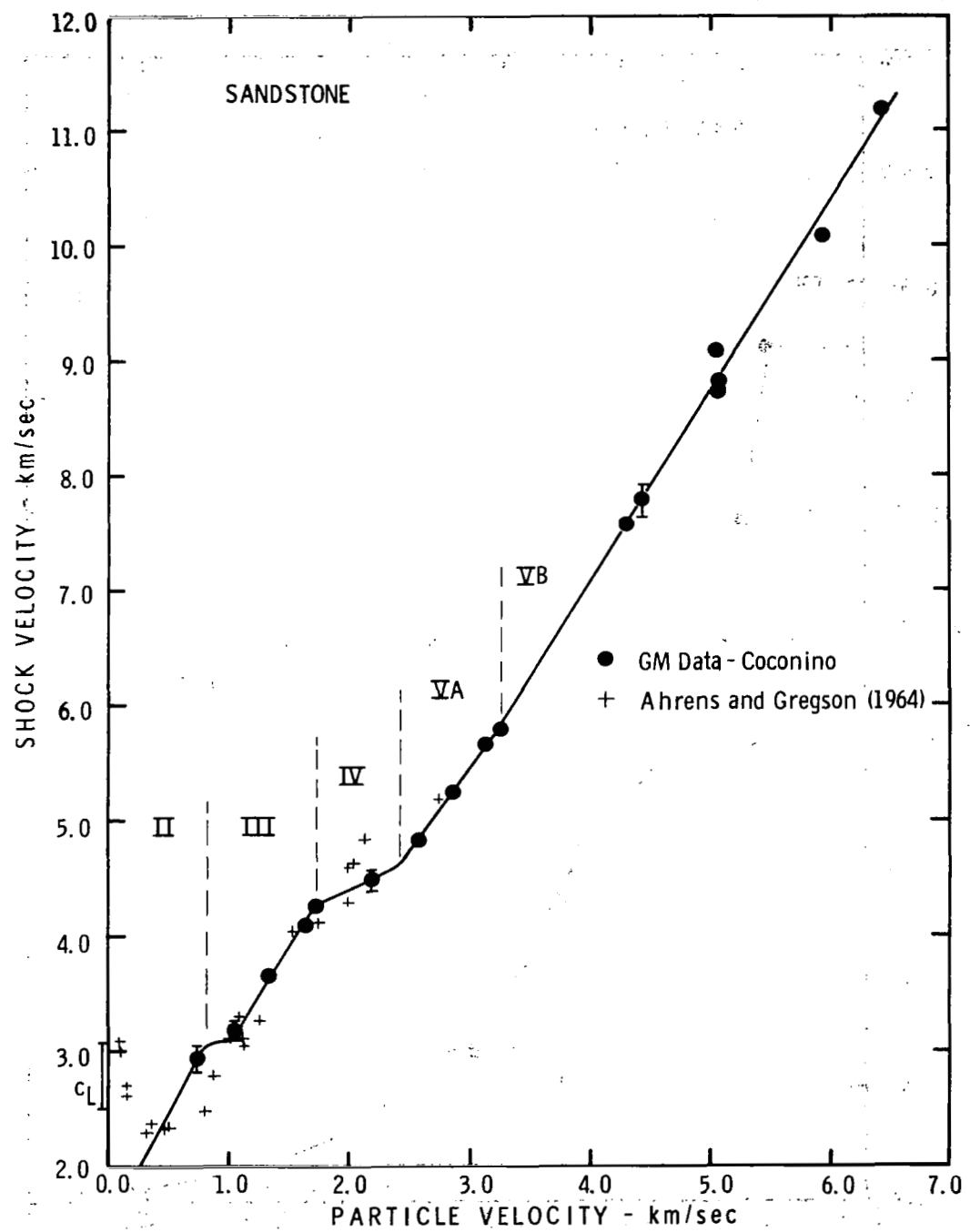


Figure 3 Shock Velocity versus Particle Velocity
Data of Sandstone

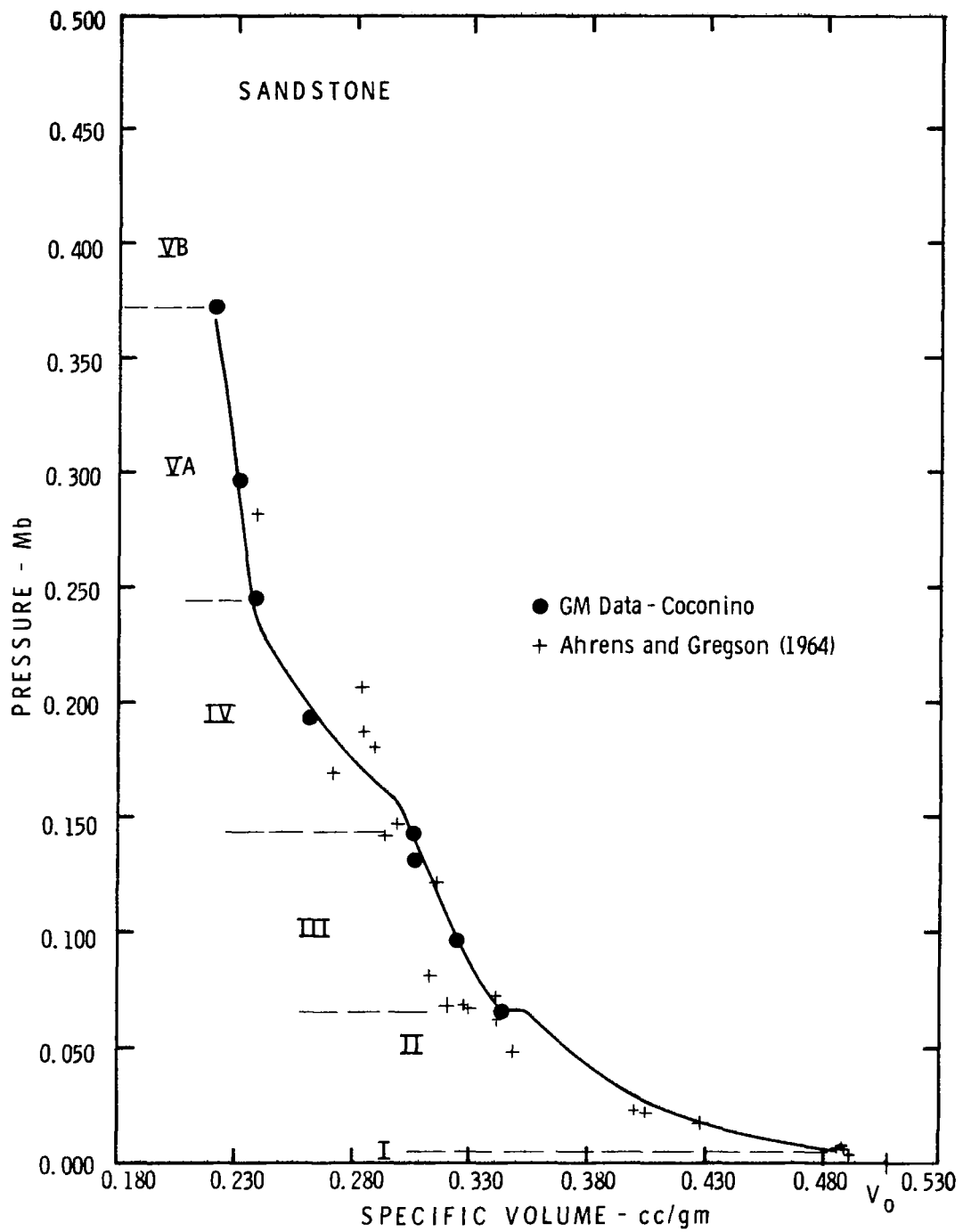


Figure 4 Hugoniot for Sandstone Data

REGION IV

$$U_s = 3.303 + 0.588 u_p \text{ km/sec}$$

$1.8 < u_p < 2.55 \text{ km/sec}$ Std. Error of $U_s = 0.126 \text{ km/sec}$

REGION VA

$$U_s = 1.172 + 1.427 u_p \text{ km/sec}$$

$2.55 < u_p < 3.35 \text{ km/sec}$ Std. Error of $U_s = 0.02 \text{ km/sec}$

REGION VB

$$U_s = 0.422 + 1.661 u_p \text{ km/sec}$$

$u_p > 3.35 \text{ km/sec}$ Std. Error of $U_s = 0.132 \text{ km/sec}$

REGIONS VA AND VB COMBINED:

$$U_s = 0.567 + 1.633 u_p \text{ km/sec}$$

$u_p > 2.3 \text{ km/sec}$ Std. Error of $U_s = 0.117 \text{ km/sec}$

Data for Coconino sandstone of Ahrens and Gregson (1964), Gregson and Grine (1963) are employed here because their material description matches ours almost identically. The only material difference is the initial density ranging from 1.96 to 2.03 gm/cm^3 versus the $1.98 \pm .03 \text{ gm/cm}^3$ average value measured for the present work.

Use of the Rankine-Hugoniot jump conditions in this work and in previous works assumes a steady state behavior. In order to determine whether steady-state conditions existed in the present experiments, several tests were performed which would exhibit non-steady waves by a variation of average shock

velocities with thickness. One such test employed a wedge of sandstone which was impacted on one face and the arrival of the shock at the tilted rear surface was recorded using a high speed rotating mirror camera. The impact conditions produced a shock in sandstone of 66 kb, which was nearly steady over the target thicknesses of 2.5 to 12.5 mm. Shock wave breakout as witnessed by an unshimmed mirror resulted in a velocity of 3.20 km/sec. The slightly ragged cut off showed only dispersion of .06 km/sec (~2%) across the wedge with the maximum velocities occurring between 5 to 9 mm. Five to 9 mm is the thickness at which most of our hugoniot measurements were performed.

The above velocity dispersion corresponds to about a .05 mm (1/2 the average grain diameter) unevenness of the shock wave front which is equivalent to the surface roughness of the target specimen.

Tests were performed with and without rear surface shims in an effort to assess their effects on recorded wave arrival times. Because particle velocity (or free surface velocity) is not measured directly by our pin technique, any difference in this parameter affected by shims would appear as data scatter. The scatter of data about the hugoniot as interpreted above is shown by the standard errors to be relatively small.

Three other tests were performed at much higher shock stresses with the more sensitive pin techniques to check for non-steady propagation. Each target was a different thickness but the impact conditions were held nearly identical. These experiments, as seen in Figure 1 and Table I, display no consistent behavior. Their ~2% scatter is larger than the experimental uncertainty and is not in the order of descending velocity with increasing thickness or vice versa. Our conclusion is that the specimen or shot reproducibility is probably no better than 2%. Within this bound, shocks appear steady over the measured data.

SECTION II

PRESSURE-VOLUME PHASE DIAGRAM FOR QUARTZ

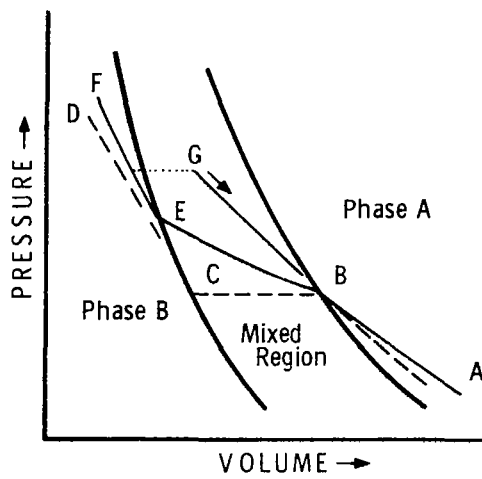
The interpretation of the hugoniot data from the previous section is employed in the following proposed description of polymorphic behavior of quartz under shock loading. Breaks or discontinuities in the sandstone and solid quartz hugoniots together with static pressure-volume data are used to estimate a P-V phase diagram for quartz. Primary concern is directed toward conditions for existence of α -quartz, coesite, stishovite phases along the hugoniot.

Inference of polymorphic behavior of materials under shock (high strain rate) loading is usually made on the basis of breaks or discontinuities in the hugoniot or shock velocity-particle velocity plot. Recovered material, shock unloading paths, and correlation with static P-V and P-T data are also used, when available, as guides in the interpretation of the high rate loading data.

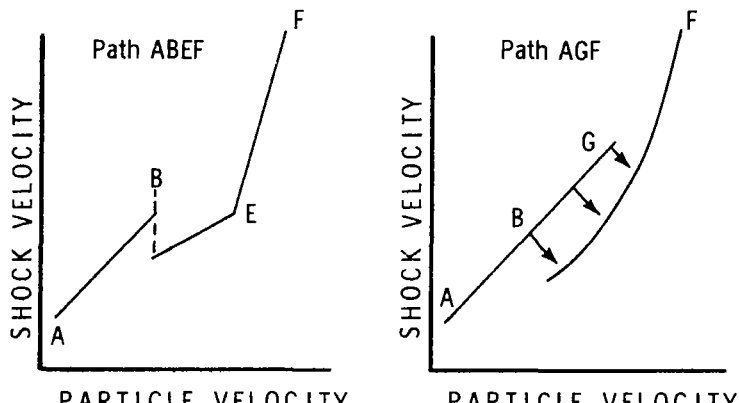
Shock behavior of idealized models of a material undergoing a polymorphic transition is discussed in detail below. Four such models are illustrated in Figures 5 and 6. These models are based on the known behavior of quartz but do not include all possible transitions, endothermic reactions, melting, phase lines such that $dP/dV > 0$, or those that are centered in a high temperature phase.

Figure 5 illustrates the shock loading of a material which has a polymorphic transition that occurs in time intervals less than

(Figure 5b) and greater than (Figure 5c) the rise time of the shock front. The heavy lines denote phase boundaries. The dashed line path ABCD, (Figure 5a) denotes the static or equilibrium states of the material undergoing a phase transition.



a.



b.

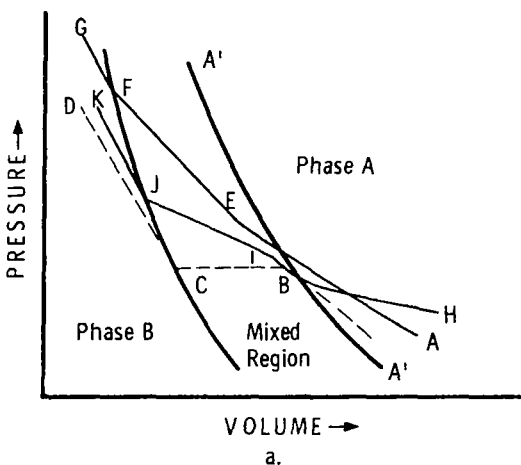
c.

Figure 5 (a) Idealized Models of Polymorphic Phase Transformation (b) Having Transition Times Less Than and (c) Greater Than the Risetime of the Shock Front

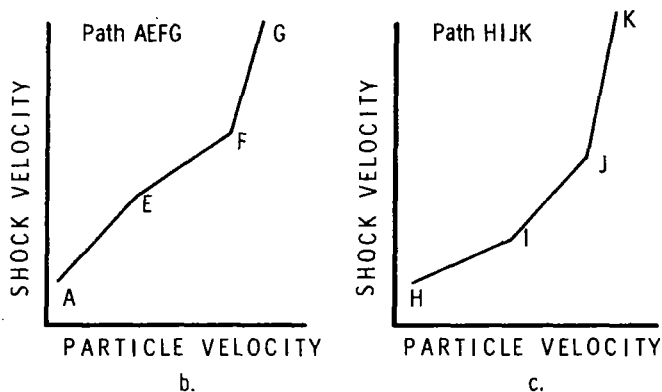
Path ABEF (Figure 5a) is typical of a material in which the transition time of the phase transformation is less than the rise time of the shock front. The area difference beneath paths ABCD and ABEF represents the non-equilibrium or "waste heat" energy between the static and dynamic loading states and results in a temperature increase at the shock front. This type of phase transition is described in some detail by Rice, McQueen and Walsh (1958). The $U_s - u_p$ plot of a material having a hugoniot represented by path ABEF is shown in Figure 5b. This is typical of a material in which a single stepped shock front occurs from A to B and again near F. A two-stepped shock front is stable in the region near B to E. Breaks or discontinuities in a $U_s - u_p$ or P-V plot for this idealized model would be an adequate indication of the onset and completion of a polymorphic transition providing other effects such as yielding can be accounted for.

Path AGF (Figure 5a) is one of several representations that is possible for a material in which the phase transformation occurs in time intervals greater than the risetime of the shock front, the difference between path ABCD and path AGF again represents the non-equilibrium energy conditions between the static and dynamic loading states. The $U_s - u_p$ plot is shown in Figure 5c. This is typical of a few materials having a large precursor decay in the double stepped wave-front from B to G. Single stepped shock fronts are stable from A to B and near F. This model illustrates one of several ways in which "time-dependent phase transitions" can exhibit a transition from one phase to another. Horie (1966) discusses such effects in some detail as does McQueen, et al. (1967). Path AGF in Figures 5a and 5c can be viewed in two ways: a pressure in excess of B is needed to drive the transition which then by stress relaxation dilates to B within the duration of the shock experiment, or the tran-

sition time is greater than the risetime of the shock front (but less than the duration of the experiment) resulting in phase A being overdriven and then relaxing. This type of behavior can be indicative of the existence of a polymorphic transition but its onset cannot be determined until the decaying double shock has traveled far enough into the material to reach a steady state propagation.



a.



b.

c.

Figure 6 (a) Idealized Models of Polymorphic Phase Transformation of a (b) Solid and (c) Porous Material Having a Transition Time Greater Than the Risetme of the Shock Front

Figure 6 illustrates two additional shock loading polymorphisms. Path AEFG (Figure 6a) is somewhat similar to path ABEF for Figure 5a except that a two stepped shock cannot occur and a single shock will be stable. Again, the difference between paths ABCD and AEFG represents the non-equilibrium condition between the static and dynamic loading states. Point E may represent an overdriven state that could relax to point B. We shall see from our experiments that the amount of overdriving and relaxation is difficult to determine and that B and E are "close" for pressure levels encountered here. Thus, a P-V or shock $U_s - u_p$ path AEFG (Figure 6a and 6b) could be an adequate indicator of phase boundaries.

Path HIJK (Figure 6a and 6c) is our model of a porous material undergoing a polymorphic phase transition. Path H to I is the regime where pore collapse occurs and where shock temperatures are expected to increase rapidly. Complete collapse of pores is generally assumed to have taken place before I but this need not always to be the case. Differences between paths ABCD and HIJK represents the non-equilibrium energy conditions as before. Point I is assumed "close" to point B because it may lie to either side of A'A' because of the competing effects of the higher temperatures available to help initiate and drive the transition and time dependency of the pore reduction. Again a single shock will be stable throughout the transition region I to J. Single shocks are found in this case because the large initial volume of the porous material allows the rayleigh line representing the "jump condition", to penetrate to every part of the hugoniot.

Figure 7 shows where models in Figures 5c, 6b and 6c have been applied to the hugoniots of porous and solid quartz and illustrate the polymorphism of quartz. (The solid quartz hugoniots was abstracted from Wackerle (1962) and Fowles (1967).)

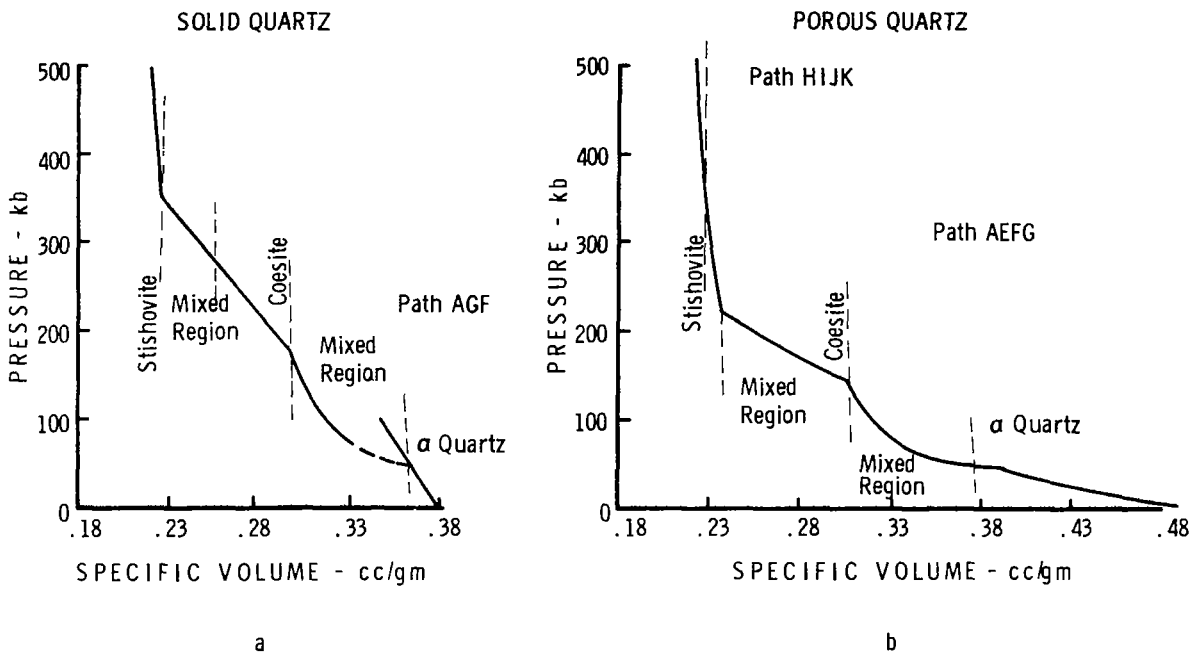


Figure 7 Interpretation of Solid and Porous Quartz Hugoniots

Data from shock unloading, shock recovery experiments and static (low strain rate) experiments are used to generate a phase diagram for quartz (Figure 8). The phase lines shown are located within limitations imposed by experimental errors of both the solid and porous hugoniot data. These boundaries delimit the P-V states at which mixed regions are totally converted for single phase and indicate only approximately the conversion temperatures. They establish nothing about the condition of mixing.

Figure 8 is a pressure-volume phase diagram for quartz and summarizes our interpretation of its overall behavior at high

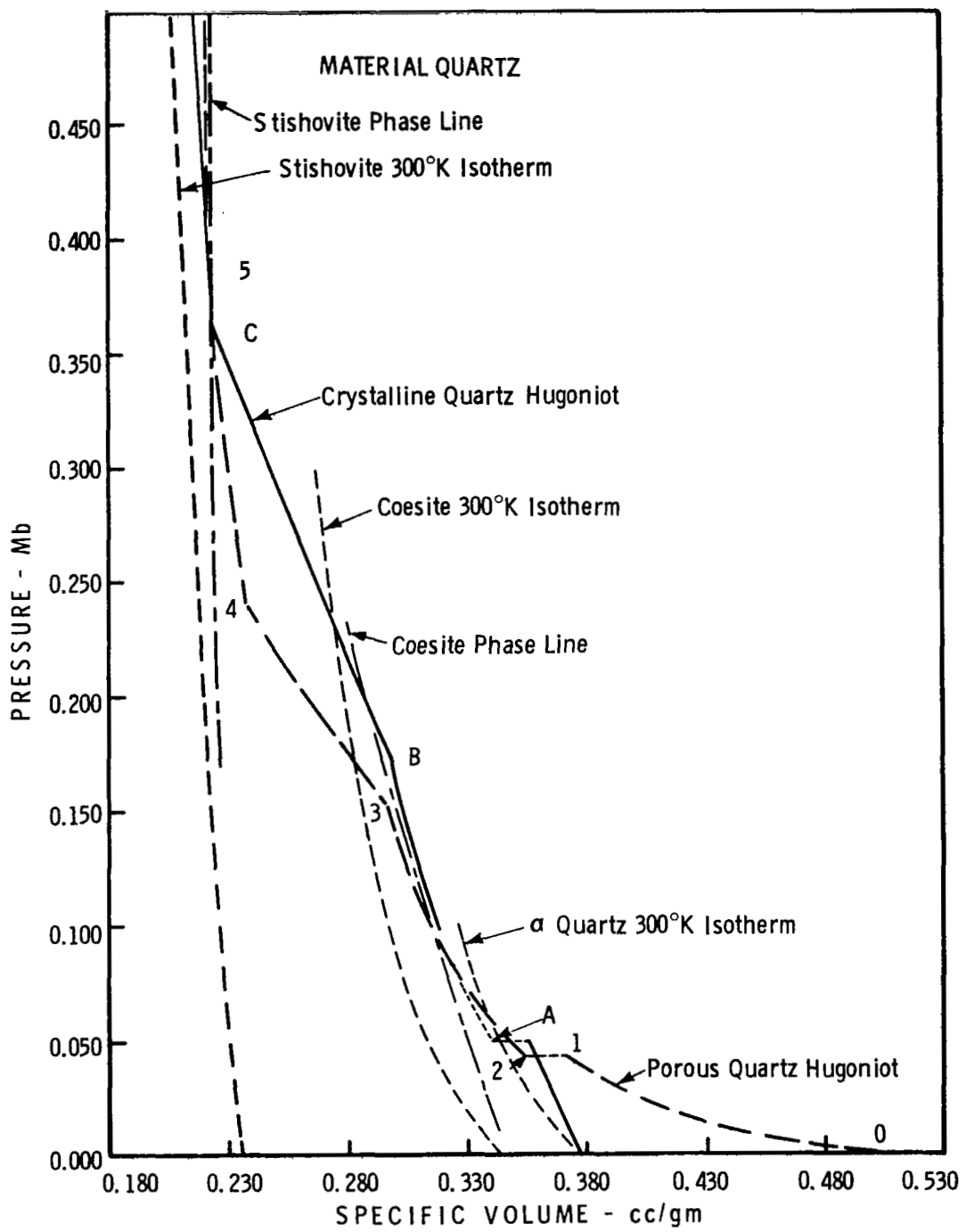


Figure 8 Pressure-Volume Phase Diagram for Quartz

pressures. The coesite to stishovite phase line is based on: the highest pressure-volume state (mean normal pressures between 360 and 385 kb) at which a change in slope occurs in the solid and porous hugoniots and a recent paper by Ahrens et al. (1970) using our data to estimate the stishovite isotherm and by McQueen, et al. (1967). The α -quartz-coesite phase line is based on the specific volume of coesite at 1 bar by Sclar, et al. (1962) and on the indicated change in slope of the sandstone hugoniot at \sim 154 kb.

The α -quartz-coesite mixed region may be evident in the solid shock wave data as the extremely large stress relaxation (Wackerle, 1962; Fowles, 1967; and Ahrens and Gregson, 1964) that takes place at or near $V = .375 \text{ cm}^3/\text{gm}$ which is commonly labeled the Hugoniot Elastic Limit (HEL). Ahrens and Duvall (1966) have made the most detailed study of this stress relaxation in quartz at its HEL but the mechanism to produce this decay is an open question. Certainly time dependent generation of even a small amount of coesite (thus placing the material in the mixed α -quartz coesite region) could result in a redistribution of shear stresses which could initiate the relaxation. The strongest argument for this mixed region is the break in the sandstone hugoniot.

The previous behavior of quartz postulated by McQueen, et al. (1963); Ahrens and Gregson (1964); and Jones, et al. 1968), was that the stress relaxation observed in quartz is the result of an unknown mechanism and that partial transformation to coesite does not occur above the HEL. They went on to postulate a direct transformation of α -quartz to stishovite at higher pressures. Coesite was not considered to exist along the hugoniot in these studies because of the extremely long time and high temperature required for the reaction to occur as observed in

static experiments. However, static phase transformations in calcite which also require long times and high temperature were found to occur within the thickness of the shock front by Ahrens and Gregson (1964) and Jones and Froula (1969). This has been noted for other phases in other materials. Breed and Venable (1968) find large time variations in shock induced phase transformations. The great shear deformation forces produced in shock fronts is usually assumed to be the driving mechanism. Dremin and Breusov (1968) have recently reviewed this aspect of dynamic processes.

Coesite is usually found as traces and small amounts in the recovered thermomorphic glass from meteor impact craters and nuclear detonations (Deribas, et al. 1966; Chao, 1967). Bunch, et al. (1968) also report shock induced structural disorder in quartz above 150 kb. Structural disorder might be evidence for partial coesite conversion followed by partial reversion of the crystal lattice by unloading. Deribas, et al. (1966) have published the only report claiming to find coesite in laboratory scale shock experiments above 150 kb. Many U.S. investigators have looked for coesite in recovered material from laboratory shock experiments but have found none (Chao, 1970).

SECTION III

TEMPERATURE CALCULATIONS

In the preceding section, static equilibrium pressure-volume states are compared with high-strain rate nonequilibrium pressure-volume states. A similar comparison can be made with pressure-temperature states. Pressure-temperature states for low strain rate equilibrium conditions are usually measured. Because shocks are of short duration ($\sim \mu\text{secs}$), temperature measurements are beyond the present state of the art.

The low-strain rate P-T phase diagram for quartz is illustrated in Figure 9. References for the numbered boundaries are listed in Table III. The quartz-coesite boundary is obtained from Holm, et al. (1967); Bell, et al. (1965); Boyd, et al. (1966); Boyd and England (1960); Yasukawa (1963); Takahaski (1963); Kitahara and Kennedy (1964); Dachille and Roy (1959); MacDonald (1956); and Griggs and Kennedy (1956). The α -quartz - β -quartz boundary is obtained from Gibson (1928), Yoder (1950), and Cohen and Klement (1967). The tridomite and cristobalite stability fields are taken from Holm et al. (1967); Stishov (1963); Sclar, et al. (1962); Bell and Boyd (1968); and Wentorf (1962). In order to generate an equivalent high strain rate P-T phase diagram for quartz, shock temperatures must be calculated.

Calculation of temperatures in solid materials is usually done by methods first outlined by Walsh and Christian (1955).

The general problem of deriving a complete P-V-T equation of state from shock data are considered by Cowperthwaite

(1966, 1969) and by Cowperthwaite and Ahrens (1967). Ahrens and Gregson (1964), have made the first calculations in sandstone and the present analysis follows their method.

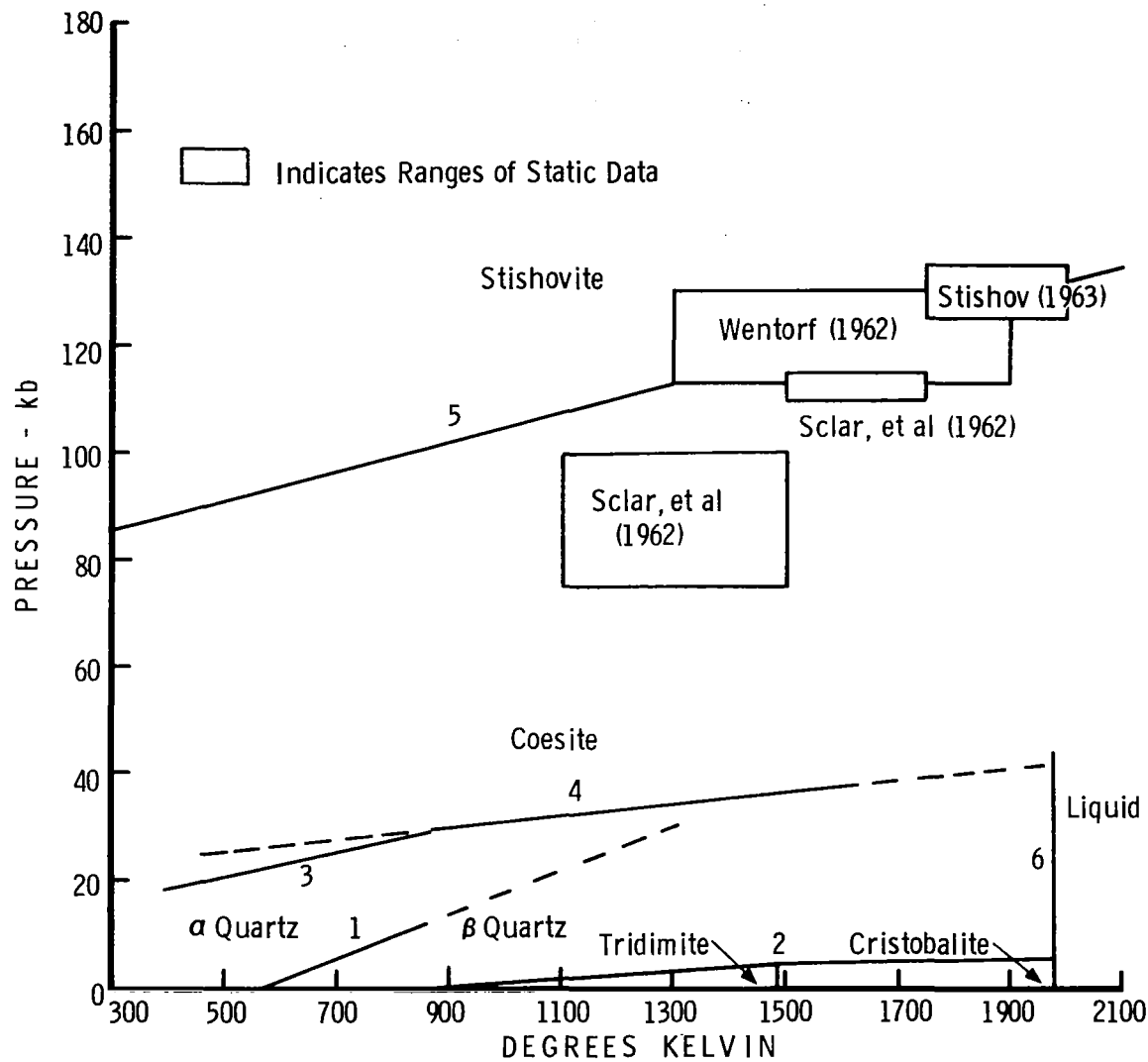


Figure 9 Low-Strain Rate Phase Diagram for Quartz

TABLE III

LOW STRAIN RATE DATA FOR EQUILIBRIUM PHASE
DIAGRAM OF QUARTZ (FIGURE 9)

1. Yoder (1950)
Gibson (1928)
Cohen and Klement (1967)
 2. Tuttle and Bowen (1958)
 3. MacDonald (1956)
Griggs and Kennedy (1956)
Dachille and Roy (1959)
 4. Boyd and England (1960)
Bell, et al. (1965)
Holm, et al. (1967)
Boyd, et al. (1966)
Yasukawa (1963)
Takahaski (1963)
Kitahara and Kennedy (1964)
 5. Holm, et al. (1967)
Stishov (1963)
Sclar, et al. (1962)
Bell and Boyd (1968)
Wentorf (1962)
 6. Mosesman and Pitzer (1941)
-

The agreement between the present calculation and that of Ahrens and Gregson (1964) is satisfactory. Error estimate based on possible variations of thermodynamic parameters made by Ahrens and Gregson (1964) indicate that these temperatures are conservative. The same arguments also hold for the present calculations. We also assume that the Gruneisen ratio, to be volume dependent and temperature independent, assuming only longitudinal lattice modes and neglecting shear

lattice and optic lattice modes. These assumptions may result in incorrectly calculated temperatures (Anderson, 1968) but no data exists to include these effects or to estimate the errors.

To calculate temperature in sandstone, the hugoniot internal energy per unit mass is partitioned into compressional energy, E_k , and thermal energy, E_t .

$$1/2 (P_1 + P_o)(V_o + V_1) = E_k + E_t$$

Where the o subscript is the initial state and the 1 subscript is the final state. V is the specific volume state and P is considered as hydrostatic pressure because of the initial small shear stress, early crushup and assumed stress equalization under shock loading. The total internal energy is obtained from the experimentally determined hugoniot; the compressional energy is determined from an isotherm. The area difference between these curves is considered to be the thermal energy.

$$E_t = \int_{T_o}^{T_h} C_v(T) dT = 1/2 (P_i - P_o)(V_o - V_i) - E_k$$

Where C_v is the specific heat capacity at constant volume.

The specific heat capacity at constant volume can be obtained from experimental measurements of C_p , the specific heat capacity at constant pressure, and from other thermodynamic parameters such as α , the volume coefficient of thermal expansion and the isothermal bulk modulus through the Gruneisens Law.

$$C_p - C_v = \alpha^2 T V^2 \left(\frac{\partial P}{\partial V}\right)_T$$

Because $(\partial P / \partial V)_T$ is estimated for small increments along the hugoniot and C_p below the Debye temperature is a function of temperature for each phase of quartz, temperature calculations are broken up into a series of regions where each of the above parameters can be handled with simplicity. Figure 10 shows the six regions which were used for temperature calculations in the shock loading of Coconino sandstone. Figures 11 and 12 show the experimental specific heat capacity data as well as the empirical fits used in the calculations.

For the elastic regime, Region I, the temperature is estimated by assuming adiabatic compression. This assumption is justified because the elastic velocity is approximately equal to the adiabatic compressional wave velocity. Thus the hugoniot and the adiabat are close. The temperature increase is thus calculated as:

$$T = T_0 \exp \frac{\Gamma (V_0 - V)}{V}$$

Where Γ is the Gruneisen coefficient and is assumed to be a constant.

For sandstone in Region I, it is difficult to obtain consistent values of Γ . From specific heat at constant pressure and volume, Γ is (Kelley 1949):

$$\Gamma = (C_v/C_p) - 1$$

Where $C_p = a + bT + cT^2$, a , b , and c are empirical constants and T is absolute temperature.

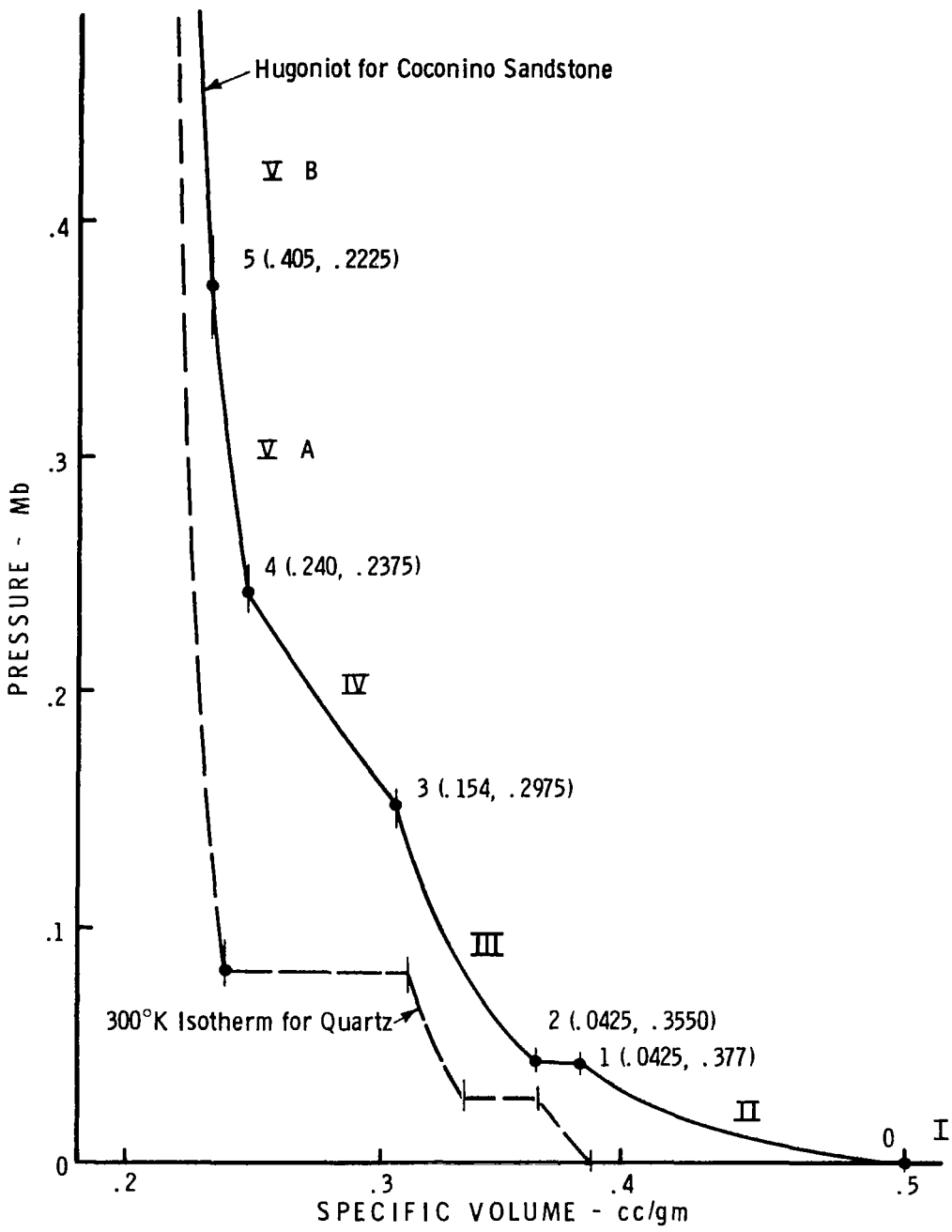


Figure 10 Coconino Sandstone Hugoniot Showing Pressure Regions Used for Temperature Calculations

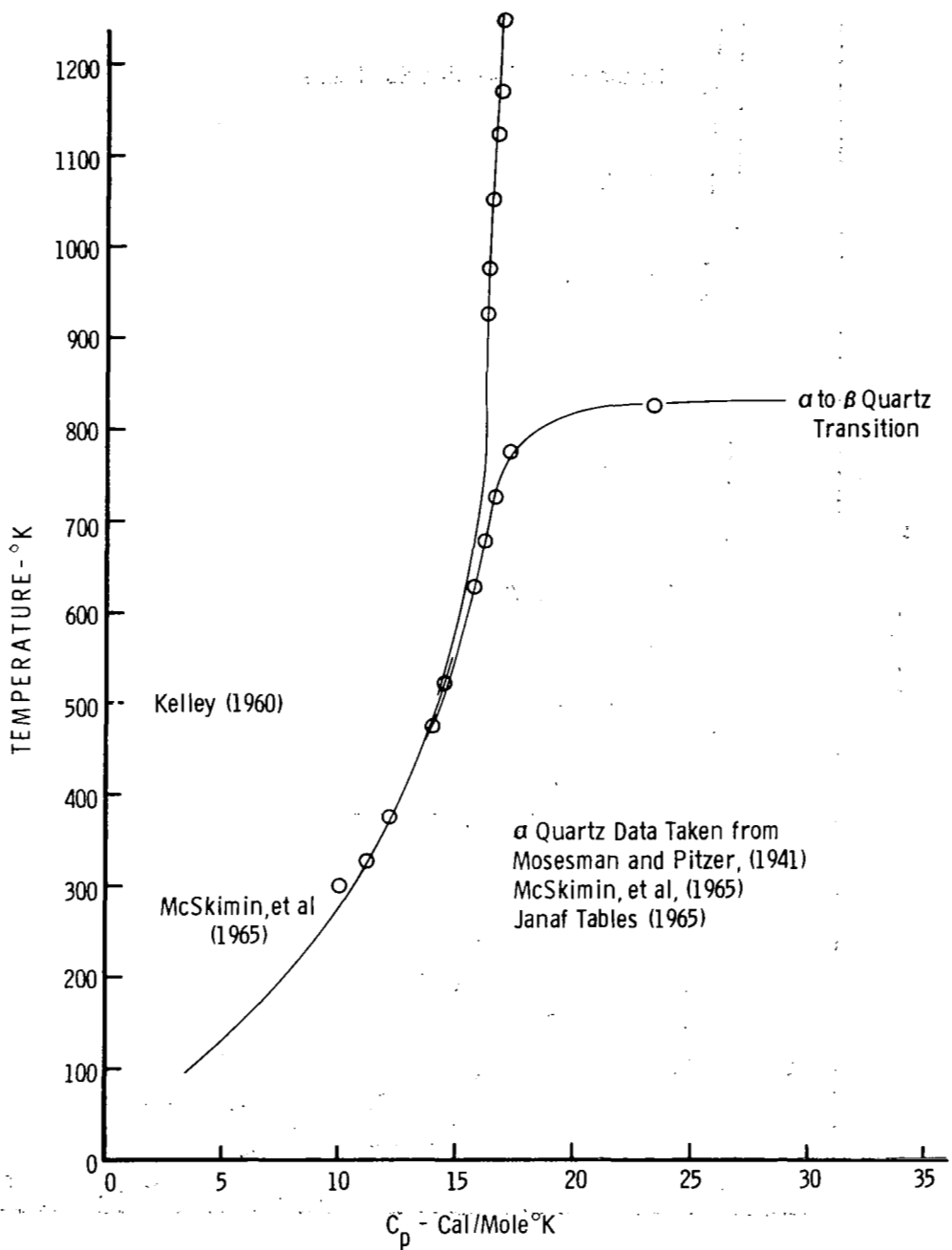


Figure 11 Specific Heat Capacity as a Function of Temperature for α -Quartz, β -Quartz, Tridimite and Cristobalite

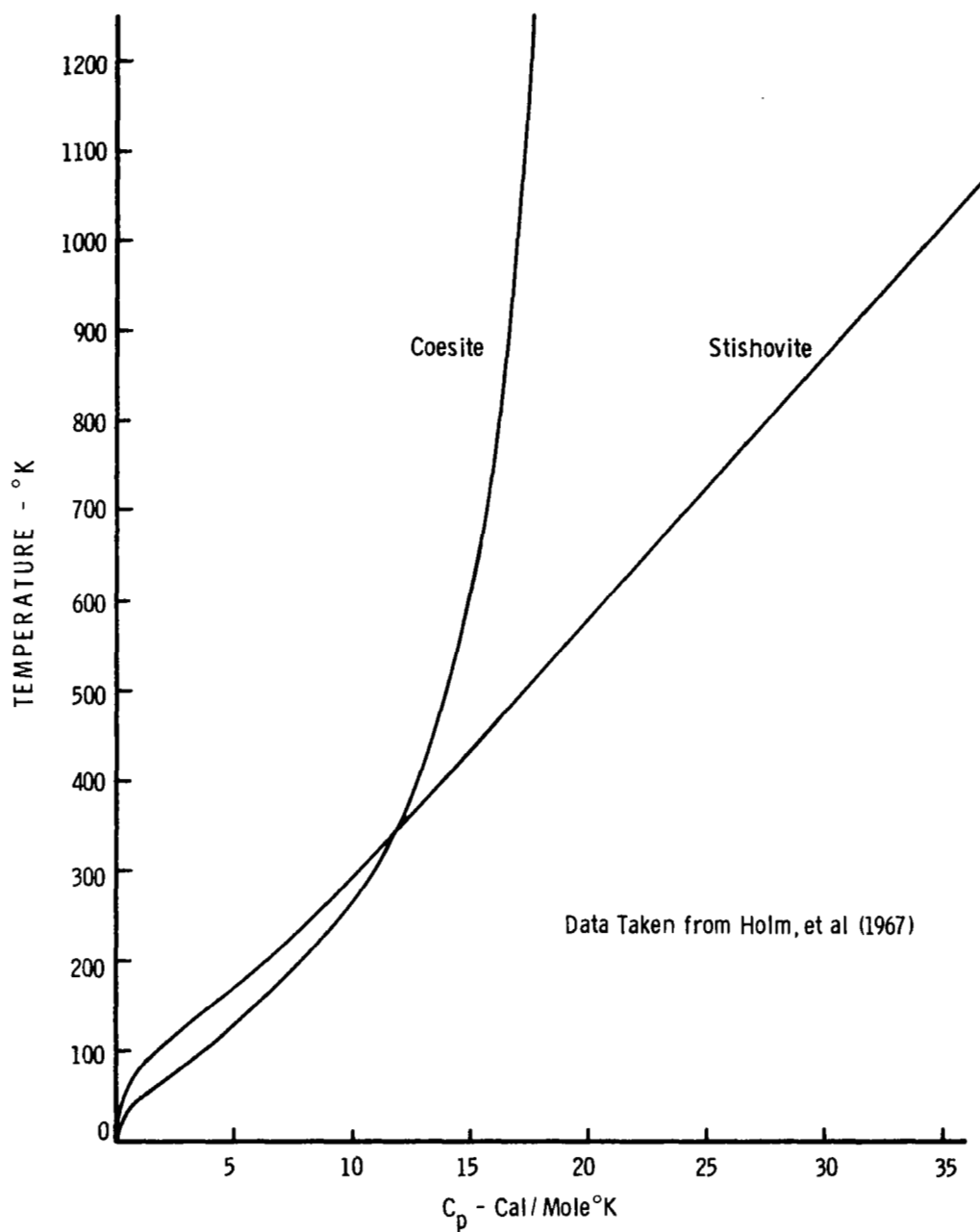


Figure 12 Specific Heat Capacity as a Function of Temperature for Coesite and Stishovite

Using the definition of Γ as:

$$\Gamma = \alpha K / C_p \rho_o$$

Where α = volumetric thermal expansion coefficient
 K = adiabatic bulk modulus
 C_p = specific heat at constant pressure
 ρ_o = initial specific density

and using handbook values (Clark, 1966), Γ has a value of 0.01 or less. Using the smaller Γ produces an increase in temperature upon compression to the HEL (4.6 kb) of a few tenths of degrees Kelvin.

Region II in sandstone is the regime between the HEL and the first break in the hugoniot. It is a region where the pores in the rock are being closed (points 0 to 1 in Figure 8). The compressional energy, E_k , is neglected because of a lack of experimental data in this pressure regime. The increase in surface energy of quartz grains during crushup has been estimated by Brace and Walsh (1962) but this energy is small compared to the compressional energy or shock energy and is also neglected for this region. Thus, all the shock internal energy is assumed to be converted into thermal energy or,

$$1/2 (P_o + P_1)(V_o - V_1) = \int_{T_o}^{T_h} C_v(T) dT$$

An initial temperature, T_o , or 300° K is assumed in all calculations of the shock temperature, T_h (neglecting temperature increase at the H.E.L.).

Specific heat capacity at constant volume for α -quartz in this temperature regime is computed incrementally from:

$$C_v = C_p - T \alpha^2 V^2 (\partial P / \partial V)_T.$$

Where T ($^{\circ}$ Kelvin) and V ($\text{cm}^3 \text{gm}^{-1}$) are average values of each increment $(\partial P / \partial V)$ along the hugoniot. A value of $1 \times 10^{-5} \text{ } ^{\circ}\text{K}^{-1}$ is used for the volume coefficient of thermal expansion, α .

Specific heat at constant pressure is taken from Figure 11 as:

$$C_p = -.13244 + 0.0448T - 3.074 \times 10^{-5} T^2$$

Where C_p has units of calories/mole $^{\circ}\text{K}$ and T is in units of $^{\circ}$ Kelvin. C_p is adjusted for an assumed linear increase in mass/unit volume from the 25% porosity condition of the sandstone to that of solid quartz over this region.

In Region III, a new energy partition was assumed because the porous material is considered to have been compressed to a solid. The internal energy was assumed to consist of a compressible and a thermal part.

$$E_{III} = \frac{(P_i - P_o)}{2} \frac{(V_o - V_i)}{} = \int_{T_o}^{T_h} C_v(T) dT + E_k$$

Where E_k is the energy of isothermal compression.

$$\text{Thus } E_k = \int_{V_o}^V - P dV.$$

If the Murnaghan form of the isotherm is assumed:

$$P = \beta \left[\left(\frac{V_0}{V} \right)^{\xi} - 1 \right]$$

Where $\beta = 42.75$ kb and $\xi = 8.390$ (Ahrens and Gregson, 1964).

The equations are solved for T_h and iterated on T_h and C_p until the temperatures agreed within a few tenths of a percent.

Calculations were performed along the Murnaghan until $V = .355 \text{ cm}^3/\text{gm}$ (point 2) was reached. This is interpreted as the mixed phase boundary between α -quartz and coesite regions. At this point, the energy from this isothermal compression using the Murnaghan form was held constant and energy was added incrementally along the flat portion of the 300°K isotherm.

$$E_k \left| \begin{array}{l} V = .355 \\ V = .375 \end{array} \right. = \int_{.395}^{.355} -\beta \left[\left(\frac{V_0}{V} \right)^{\xi} - 1 \right] dV + \int_{.355}^{.3225} PdV$$

where $\beta = 42.75$ kb and $\xi = 8.390$. Calculations have now been performed along the isotherm to 42.5 kb and 0.3225 gm/cc.

The region from 42.5 kb to 80 kb along the 300°K isotherm is the region of complete transformation to coesite. Because little experimental evidence of the isothermal compression of coesite exists, we assumed a Murnaghan form using the same ξ as quartz and replacing β_c with the isothermal bulk modulus of quartz. The total energy is now:

$$E_k \left| \begin{array}{l} V = .2975 \\ V = .39 \end{array} \right. = \int_{.39}^{.3550} -\beta \left[\left(\frac{V_0}{V} \right)^\xi - 1 \right] dV +$$

$$\int_{.3550}^{.3225} dV + \int_{.3225}^{.2975} -\beta_c \left[\left(\frac{V_0}{V} \right)^\xi - 1 \right] dV$$

The specific heat capacities at constant pressure for α -quartz and coesite in Region III are:

$$C_p \left| \begin{array}{l} \alpha\text{-quartz} \end{array} \right. = -.1324 + .0448 T - 3.074 \times 10^{-5} T^2$$

(200°K to 750°K)

$$C_p \left| \begin{array}{l} \beta\text{-quartz} \end{array} \right. = 14.65 + .00177 T$$

(750°K to 1140°K)

and

$$C_p \left| \begin{array}{l} \text{coesite} \end{array} \right. = 3.190 + .0297 T - 1.614 \times 10^{-5} T^2$$

(200°K to 920°K)

The two equations for quartz are necessary to bridge the α - β quartz transition at about 850°K. A linear mixing law between quartz and coesite is assumed in this region.

$$C_p \left| \begin{array}{l} \text{coesite} \end{array} \right. = 15.8115 + 1.132 \times 10^{-3} T$$

(920°K to 3000°K)

The material transforms from 100% quartz at the beginning of

Region III to 100% coesite at the end of Region III. An average specific heat capacity at constant pressure is calculated at each $(\partial P/\partial V)$ interval of the calculation by assumming appropriate mixtures of the two C_p 's. A C_v is then calculated and used in the energy partition equation to calculate shock temperature.

Regions IV and VA are the mixed regions for the transformation from coesite to stishovite. A linear mixing law for the corresponding specific heats at constant pressure results in temperatures which we consider too low. Thus Region IV was assumed to represent the region where 50% of the material is transformed to stishovite. Region VA represents the region where the remaining 50% of the material is transformed to stishovite. The appropriate specific heat at constant pressure is shown in Figure 12.

Likewise, the energy from isothermal compression is the sum of the previous energies plus the flat region from $V = .2975$ to $V = .2275$ and a Murnaghan fit to the stishovite region.

$$E_k \left| \begin{array}{l} V = .2225 \\ \\ V = .39 \end{array} \right. = E_k \left| \begin{array}{l} .2975 \\ .39 \end{array} \right. + \int_{.2975}^{.2375} -PdV + \int_{.2375}^{.2225} -PdV +$$

$$\int_{.2275}^{.2225} -\beta_s \left[\left(\frac{V_0}{V} \right)^{\xi_s} - 1 \right] dV$$

We used the isothermal bulk modulus (β_s) and its first derivative (ξ_s) for stishovite as given by Ahrens, et al. (1970)

to fit the simplified Murnaghan equation to the stishovite region rather than the Birch-Murnaghan form with higher order corrections as given by Ahrens, et al. (1970). This was done to simplify the integrations and because any differences between the two approaches seemed small compared with approximations and estimations already made to reach this point in the calculations.

Region VB is the region where material has been completely transformed to stishovite. The C_p and E_k used in the temperature calculations is the same as previously given.

Similar calculations are made using the solid quartz hugoniot. The various regions of the hugoniot and the 300°K isotherm are shown in Figure 13 and correspondingly in Figure 8. A discussion of the calculations will not be made but follows along the same lines as for the sandstone. Several comments are in order about the specific form of the solid quartz hugoniot. First, the HEL is taken as ~ 45 kb which is close to an asymptotic value of the HEL decay that is observed in solid quartz. This is interpreted by us to be a shock steady state equilibrium condition for the onset of the α -quartz/mixed region. Second, calculations are made for α -quartz transforming, directly to stishovite (B to C' in Figure 14) as well as the α -quartz-coesite-stishovite (B to C) as was done for sandstone. The α -quartz to stishovite seems a more probable transformation within the shock front of laboratory experiments. The α -quartz-coesite-stishovite transitions are used because they appear to represent equilibrium conditions along the whole hugoniot. These two possible transformation processes should bound the actual transformation temperature conditions. Thirdly, because of the high resolved shear stress in α -quartz, a mean normal stress is computed through Poisson's ratio and the hugoniot stress.

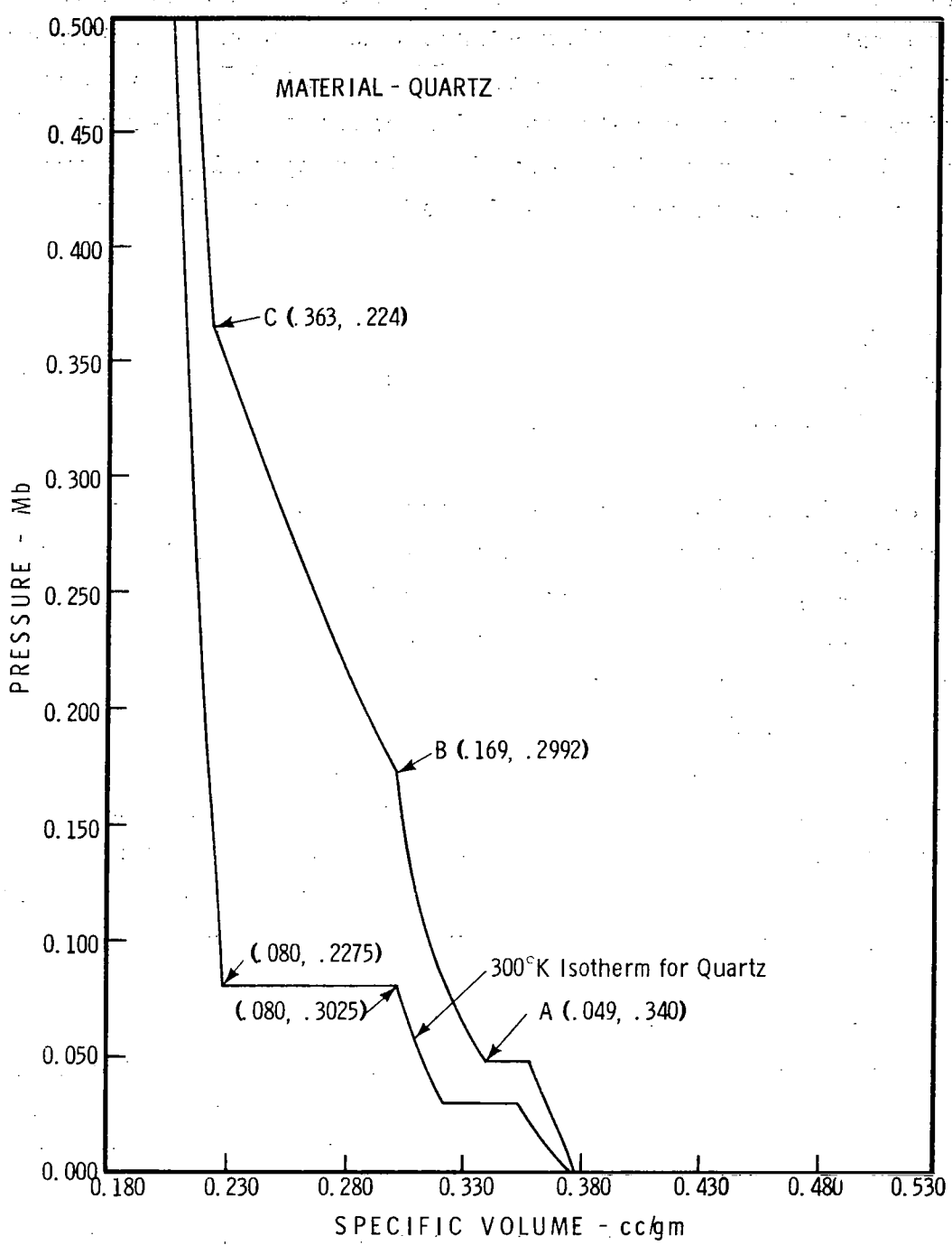


Figure 13 Solid Quartz Hugoniot Showing Pressure Regions Used for Temperature Calculations

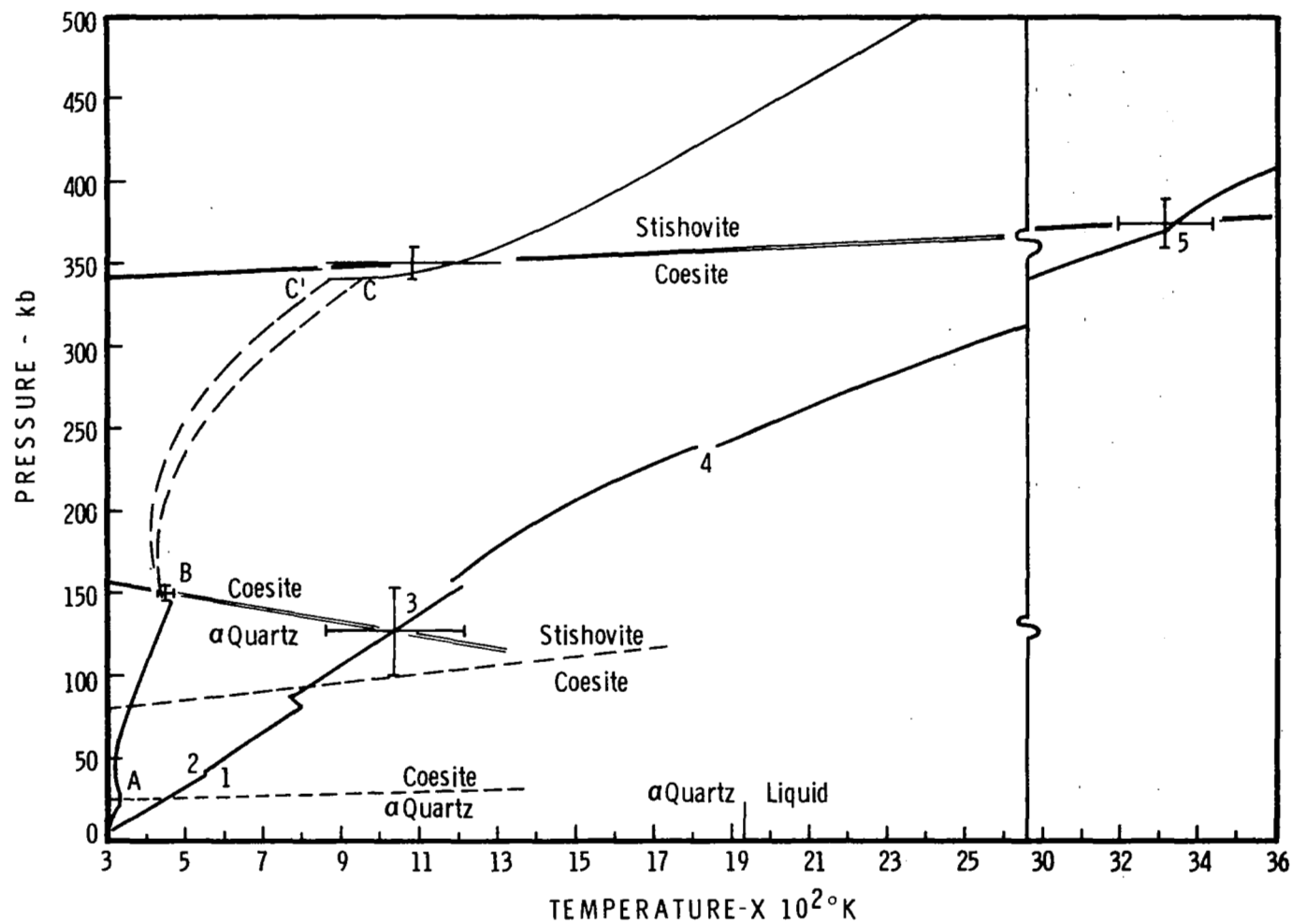


Figure 14 High Strain Rate Phase Diagram for Quartz

CONCLUSIONS

Figure 14 illustrates the high strain rate phase boundaries for α -quartz-coesite and coesite-stishovite concluded from our interpretation of the hugoniot data and estimated iso-therms. The doubled lines represent the completed transition under shock loading and the dash lines represent the hydrostatic transitions. Error estimates are also shown. Lettered and numbered points in the figure correspond to discontinuities in the hugoniots shown in Figure 8. Discontinuities in the hugoniot temperature curves result from the simplifications of the hugoniots and isotherms.

An estimate of the range of strain rates obtained in our shock wave experiments is from $\sim 3 \times 10^2$ to 1.3×10^{11} /sec. Strain rates for hydrostatic experiments are normally in the range from 10^{-6} to 10^{-3} /sec. An obvious effect of the 14 to 17 orders of magnitude increase in strain rate on the polymorphism of quartz is a significant shift in the pressure-temperature plane of the phase boundaries of coesite and stishovite.

Shock wave studies of quartz have application in at least two areas of geophysics. The first concerns the thermodynamic states of minerals present in the earth's mantel. Accurately measured P-V states assist in more accurate determinations of the thermodynamic properties and density states of quartz polymorphs and thus help in determining the mineral assemblages that might be possible in the earth's mantel.

The second area concerns meteorite craters and interpretations of the physical conditions that existed at impact. Many present

studies of such impacts base description of the P-V-T states on hydrostatic phase diagrams. The change in phase boundaries with strain rate as illustrated here might lead to a reevaluation of such interpretations. Because of the effect of strain rate as shown in Figure 14, an upper and lower limit may be established for the stability of quartz in the impact process. Previous interpretations of quartz should be viewed as only a lower bound.

APPENDIX

APPENDIX

HUGONIOT STANDARDS

It has been found practical to induce ultra-high stresses by causing a high density metal plate to strike a target of the material of interest at high velocities. The basis of the present technique using a light gas gun as a projector is to impact sandstone targets with a flat plate of OFHC copper or Fansteel-77 (a tungsten alloy). The hugoniot state in the target is measured by recording the impactor velocity prior to impact and the shock velocity induced in the specimen. Computation of the resultant volume or particle velocity requires, in addition to the above measurements, knowledge of a hugoniot equation of state of the impactor material (McQueen, et al., 1967).

The hugoniot equations for the metals used in this program have been measured in this laboratory and are listed below.

OFHC Copper:

$$U_s = 3.964 + 1.463 u_p \text{ (km/sec)}$$

RMS Deviation of $U_s = \pm .009 \text{ km/sec}$

Fansteel-77:

$$U_s = 4.008 + 1.262 u_p \text{ (km/sec)}$$

RMS Deviation of $U_s = \pm .021 \text{ km/sec.}$

A more complete description of the measurements on these metals may be found in Isbell, Shipman and Jones (1968).

LITERATURE CITED

Ahrens, T. J. and Duvall, G. E., "Stress Relaxation Behind Elastic Shock Waves in Rocks", J. Geophys. Res., Vol. 71, No. 18, p. 4349-4360, 15 Sept. 1966.

Ahrens, T. J. and Gregson, Jr., V. G., "Shock Compression of Crustal Rocks; Data for Quartz, Calcite and Plagioclase Rocks", J. Geophys. Res., Vol. 69, No. 22, p. 4839-4874, 15 Nov. 1964.

Ahrens, T. J., Takahaski, T. and Davies, G. F., "A Proposed Equation of State of Stishovite", J. Geophys. Res., Vol. 15, No. 2, p. 310-316, 10 Jan. 1970.

Anderson, O. L., Comments on the Negative Pressure Dependence of the Shear Modulus Found in Some Oxides", J. Geophys. Res., Vol. 73, p. 7707-7712, 1968.

Bell, P. M., Simmons, G. and Hays, J. F., "Shearing Squeezer Experiments with Quartz and Coesite", Carnegie Inst., Wash. Yr. Book, Vol. 64, p. 141-144, 1965.

Bell, P. M. and Boyd, F. R., "Phase Equilibrium Data Bearing on the Pressure and Temperature of Shock Metamorphism", 43-50 in Shock Metamorphism of Natural Materials, edited by B. M. French and N. M. Short, Mono Book Corp., Baltimore, Md., 1968.

Boyd, F. R., Bell, P. M., England, J. L. and Gilbert, M. C., "Pressure Measurements in Single Stage Apparatus", Carnegie Inst. Wash. Yr. Book, Vol. 65, p. 410-414, 1966.

Boyd, F. R. and England, J. L., "The Quartz-Coesite Transition", J. Geophys. Res., Vol. 65, No. 2, p. 749-756, Feb., 1960.

Breed, B. R. and Venable, D., "Dynamic Observations of the Course of a Shock-Induced Polymorphic Phase Transition in Antimony", J. Appl. Phys., Vol. 39, p. 3222-3224, June, 1968.

Bunch, T. E., Cohen, A. J. and Dence, M. R., "Shock-Induced Structural Disorder in Plagioclase and Quartz", in Shock Metamorphism of Natural Materials, edited by B. M. French and N. M. Short, Mono Book Corp., Baltimore, Md., 1968.

Brace, W. F. and Walsh, J. B., "Some Direct Measurements of the Surface Energy of Quartz and Orthoclase", Am. Mineralogist, Vol. 46, p. 1111-1122, 1962.

Chao, E. C. T., "Shock Effects in Certain Rock-Forming Minerals", Science, Vol. 156, p. 192-202, 1967.

Chao, E. C. T., "Impact Metamorphism", in Res. in Geochemistry, Vol. 2, editor P. H. Abelson, John Wiley & Sons, Inc. N. Y., 1967.

Chao, E. C. T., Private Communication, April, 1970.

Clark, Jr., S. P., editor, Handbook of Physical Constants, Geo. Soc. of Am., Memoir 97, 1966.

Cohen, L. H. and Klement, Jr., W., "High-Low Quartz Inversion: Determination to 35 kilobars", J. Geophys. Res., Vol. 72, No. 16, p. 4245-4251, 15 Aug. 1967.

Cowperthwaite, M., "Significance of Some Equations of State obtained from Shock-Wave Data", Am. J. Phys., Vol. 34, No. 11 p. 1025-1030, Nov., 1966.

Cowperthwaite, M., "Relationships Between Incomplete Equations of State", J. Franklin Inst., Vol. 287, No. 5, p. 379-387, May, 1969.

Cowperthwaite, M. and Ahrens, T. J., "Thermodynamics of the Adiabatic Expansion of a Mixture of Two Phases", Am. J. Phys., Vol. 35, No. 10, p. 951-955, Oct., 1967.

Dachille, F. and Roy, R., "High Pressure Region of the Silica Isotypes", Z. Krist., Vol. III, p. 451-461, 1959.

Deribas, A. A., Dobretsov, N. L., Kudinov, V. M. and Zyuzin, N. I., Doklady Akad. Nauk SSR, Vol. 168, p. 665, 1966.

Dremin, A. N. and Breusov, O. N., "Processes Occuring in Solids Under the Action of Powerful Shock Waves", Russian Chemical Rev., Vol. 37, No. 5, p. 392-402, 1968.

Fowles, G. R., "Dynamic Compression of Quartz", J. Geophys. Res., Vol. 72, No. 22, p. 5729-5742, 15 Nov. 1967.

Fowles, G. R., "Determination of Constitutive Relations from Plan Wave Experiments", J. Appl. Phys., Vol. 41, 1970.

Gibson, R. D., "The Influence of Pressure on the High-Low Inversion of Quartz", J. Phys. Chem., Vol. 32, p. 1197-1205, 1928.

Gregson, V. G. and Grine, D. R., "Vela-Uniform Dynamic Properties of Rocks", Stanford Research Inst., Contract No. AFL9 (604) 8419 for Advanced Research Projects Agency, 15 Aug. 1963.

Griggs, D. T. and Kennedy, G. C., "A Simple Apparatus for High Pressures and Temperatures", Amer. J. Sci., Vol. 254, p. 722-735, 1956.

Holm J. L., Kleppa, O. J. and Westrum, Jr., E. F., "Thermodynamics of Polymorphic Transformations in Silica. Thermal Properties from 5 to 1070°K and Pressure-Temperature Stability Fields for Coesite and Stishovite", Geoschemical et Cosmochemica Acta, Vol. 31, p. 2289-2307, 1967.

Horie, Y., "The Kinetics of Phase Change in Solids by Shock Wave Compression", PhD. Thesis, Dept. of Physics, Washington State University, Pullman, Washington, 1966.

Isbell, W. M., Shipman, F. H. and Jones, A. H., "Hugoniot Equation of State Measurements for Eleven Materials to Five Megabars", MSL-68-13, General Motors Corporation, Manufacturing Development, Materials and Structures Laboratory, Warren, Michigan, 1968.

James, O. B., "Jadeite: Shock-Induced Formation Frame Oligoclase, Ries Crater, Germany", Science, Vol. 165, p. 10050-1008, 1969.

Janaf Thermochemical Tables, Clearinghouse for Federal Scientific and Technical Information, 1965.

Jones, A. H. and Froula, N. H., "Uniaxial Strain Behavior of Four Geological Materials to 50 Kilobars", MSL-68-19, and DASA-2209, General Motors Corporation, Manufacturing Development, Materials and Structures Laboratory, Warren, Michigan, Contract No. DA-49-146-XZ-544, Defense Atomic Support Agency, March, 1969.

Jones, A. H., Isbell, W. M., Shipman, F. H., Perkins, R. D., Green, S. J. and Maiden, C. J., "Materials Properties Measurements for Selected Materials", MSL-68-19, Interim Report, Contract No. NAS2-3427, April, 1968.

Kelley, K. K., "Contribution to the Data on Theoretical Metallurgy", U.S. Dept. of the Interior, U.S. Bureau of Mines, Bull. 476, 1949.

Kelley, K. K., "Contributions to the Data on Theoretical Metallurgy XIII, High Temperature Heat-Content, Heat-Capacity, and Entropy Data for the Elements and Inorganic Compounds", U.S. Bureau of Mines, Bull. 584, 1960.

Kitahara, S. and Kennedy, G. C., "The Quartz Coesite Transition", J. Geophys. Res., Vol. 69, p. 5395-5400, 1964.

MacDonald, G. J. F., "Quartz-Coesite Stability, Relations at High Temperatures and Pressures", Am. J. Sci., Vol. 254, p. 713-721, 1956.

McQueen, R. G., Fritz, J. N. and Marsh, S. P., "On the Equation of State of Stishovite", J. Geophys. Res., Vol. 68, p. 2319-2322, 1963.

McQueen, R. G., Marsh, S. P. and Carter, W. J., High Dynamic Pressure, Paris, 1967.

McQueen, R. G., Marsh, S. P. and Fritz, J. N., "Hugoniot Equation of State Twelve Rocks", J. Geophys. Res., Vol. 72, No. 20, p. 4999-5036, 15 Oct. 1967.

McSkimin, H. J., Andreatch, Jr., P. and Thurston, R. N., "Elastic Moduli of Quartz versus Hydrostatic Pressure at 25° and -195.8°C", J. Appl. Phys., Vol. 36, No. 5, p. 1624-1632, May, 1965.

Mosesman, M. A. and Pitzer, K. S., "Thermodynamic Properties of the Crystalline Forms of Silica", J. Am. Chem. Soc., Vol. 63, p. 2348-2356, Sept., 1941.

Rice, M. H., McQueen, R. G. and Walsh, J. M., "Compression of Solids by Strong Shock Waves", Vol. 6 of Solid State Physics eds. F. Saitz and D. Turnbull, Academic Press, Inc., New York, 1958.

Ringwood, A. E., Reid, A. F. and Wadsley, A. D., "High Pressure $KAlSi_3O_8$, an Aluminosilicate with Sixfold Coordination", Acta Cryst., Vol. 23, p. 1093, 1967.

Ringwood, A. E., Reid, A. F. and Wadsley, A. D., "High Pressure Transformation of Alkali Aluminosilicates and Aluminogermanates", Earth Planet Sci. Lett., Vol. 3, p. 38, 1967.

Sclar, C. B., Young, A. P., Garrison, L. C. and Schwartz, C. M., "Synthesis and Optical Crystallography of Stishovite, A Very High Pressure Polymorph of SiO_2 ", J. Geophys. Res., Vol. 67, No. 10, p. 4049-4054, Sept., 1962.

Shipman, F. H., Isbell, W. M. and Jones, A. H., "High Pressure Hugoniot Measurements for Several Nevada Test Site Rocks", MSL-68-15, General Motors Corporation, Manufacturing Development, Materials and Structures Laboratory, Warren, Michigan, 1968.

Stishov, S. M., "Equilibrium Line Between Coesite and Rutile-Like Modification of Silica", Doklady, Acad. Nauk SSR, Vol. 148, p. 1186-1188, 1963.

Takahaski, T., "Factors Influencing Pressures in Multi-Anvil Devices", in High Pressure Measurement, edited by Giardini and Lloyd, p. 240-244, Butterworths, Washington, D. C., 1963.

Wackerle, J. H., "Shock Wave Compression of Quartz", J. Appl. Phys., Vol. 33, p. 922-937, 1962.

Walsh, J. M. and Christian, R. H., "Equation of State of Metals from Shock Wave Measurements", Phys. Rev., Vol. 97, p. 1544-1556, 1955.

Wentorf, R. H., Jr., "Stishovite Synthesis", J. Geophys. Res., Vol. 67, p. 3648, 1962.

Yasukawa, K., "The Phase Transition Between Quartz and Coesite", Mem. Coll. Sci. Univ. Kyoto, B., Vol. 30, p. 121-145, 1963.

Yoder, Jr., H. S., "High Low Quartz Inversion Up to 10,000 Bars", Trans. Am. Geo. Union, Vol. 31, p. 827-835, 1950.